CHEMISTRY OF MATERIALS

pubs.acs.org/cm

Article

Tuning the Piezoresistive Behavior of Graphene-Polybenzoxazine Nanocomposites: Toward High-Performance Materials for Pressure Sensing Applications

Published as part of the Chemistry of Materials virtual special issue "In Honor of Prof. Clement Sanchez".

Stefania Vitale, Hugo Puozzo, Shamil Saiev, Leïla Bonnaud, Antonio Gaetano Ricciardulli, Artur Ciesielski,* David Beljonne,* and Paolo Samorì*

Cite This: *Chem. Mater.* 2023, 35, 6909−6919

Read Online

ACCESS | Metrics & More | Article Recommendations | Supporting Information

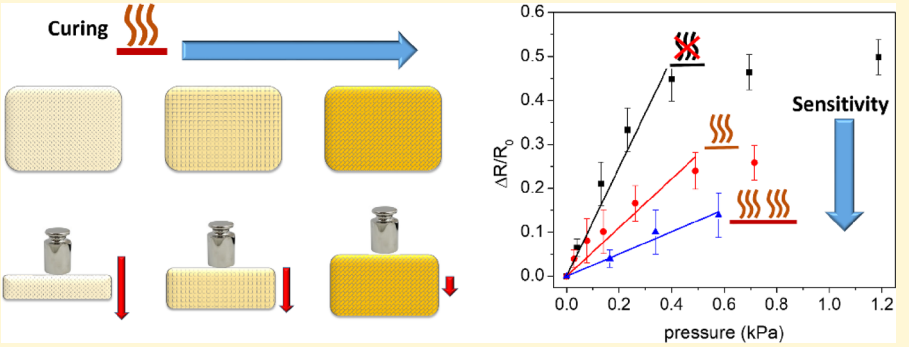

ABSTRACT: Flexible piezoresistive pressure sensors are key components in wearable technologies for health monitoring, digital healthcare, human−machine interfaces, and robotics. Among active materials for pressure sensing, graphene-based materials are extremely promising because of their outstanding physical characteristics. Currently, a key challenge in pressure sensing is the sensitivity enhancement through the fine tuning of the active material's electro-mechanical properties. Here, we describe a novel versatile approach to modulating the sensitivity of graphene-based piezoresistive pressure sensors by combining chemically reduced graphene oxide (rGO) with a thermally responsive material, namely, a novel trifunctional polybenzoxazine thermoset precursor based on tris(3-aminopropyl)amine and phenol reagents (PtPA). The integration of rGO in a polybenzoxazine thermoresist matrix results in an electrically conductive nanocomposite where the thermally triggered resist's polymerization modulates the active material rigidity and consequently the piezoresistive response to pressure. Pressure sensors comprising the rGO-PtPA blend exhibit sensitivities ranging from 10^{-2} to 1 kPa^{-1}, which can be modulated by controlling the rGO:PtPA ratio or the curing temperature. Our rGO-PtPA blend represents a proof-of-concept graphene-based nanocomposite with on-demand piezoresistive behavior. Combined with solution processability and a thermal curing process compatible with large-area coatings technologies on flexible supports, this method holds great potential for applications in pressure sensing for health monitoring.

INTRODUCTION

Global interest in wearable technologies steers the progress in flexible electronics, which is indispensable to unlocking the full potential of wearables in technological areas currently under the spotlight, such as health monitoring and digital healthcare,[1−3] human−machine interfaces,[4,5] robotics,[6] and Internet of (Medical) Things.[7,8] In this context, the rapid pace of flexible pressure sensors in the past few years plays a key role.[9] To overcome the limitations of traditional pressure sensors based on metals and semiconductors, e.g., rigidity, high production costs, and cumbersome processability,[10] research efforts are currently focused on the development of novel systems comprising flexible components and featuring superior mechanical properties and cost-effective and scalable production and processing. Various nanomaterial-based systems (including MoS_2,[11] MXene,[12] and gold nanoparticles)[13] are being explored as candidates for pressure-sensitive active materials that, once integrated into a device with appropriate flexible substrates and electrodes, can ensure high sensitivity, durability, and fulfillment of all the aforementioned character-

Received: May 16, 2023
Revised: August 2, 2023
Published: August 17, 2023

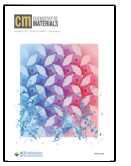

istics.[14,15] Among them, graphene and its derivatives are particularly appealing since they display excellent electrical and mechanical properties, high flexibility, and lightweight, rendering graphene-based materials particularly suitable for application in pressure sensing.[16] One common approach to integrating graphene-based materials in a pressure sensor consists in their incorporation into flexible or elastic substrates, such as rubbers,[17,18] fibers,[19,20] fabrics,[21,22] or polymer matrices.[18,23,24] With this approach, various types of pressure sensors featuring different structures have been integrated into capacitive,[25,26] piezorestistive,[15,16] and piezoelectric[27,28] sensors. Piezoresistive sensors are particularly promising for technological implementation, given their simple sensing mechanism and design, low power consumption, and easy readout.[15,16,29]

For applications in flexible electronics, a high sensitivity in the low-pressure regime (i.e., 0.1−10 kPa, compatible with tactile perception) is crucial. In piezoresistive devices, the sensing mechanism relies on variations of the active material electrical resistance (tunneling resistance or contact resistance); briefly, the application of compressive stresses causes changes in the material microstructure and consequently variations in the electrically conductive pathways within the sensing material.[16,29] Hence, the fabrication of microstructured networks featuring high porosity or geometrical arrays of sensing material is an attractive approach for tailoring the device sensitivity.[30−36] However, time-consuming and high-cost processes are usually needed to fabricate such devices. Furthermore, the fixed microstructured network translates in a pressure sensor with a given sensitivity, which is fixed by the electro-mechanical properties of the chosen network and hence cannot be tuned (unless by preparing another material with a different microstructure). Responsive switchable materials (i.e., materials capable of undergoing significant changes in their physical or chemical properties as a result of exposure to external stimuli (e.g., pH, light, heat)) appear particularly appealing in this context.[37] A promising strategy for conveniently tailoring the sensitivity of piezoresistive sensors consists in incorporating in the sensing element a material possessing on-demand tunable mechanical properties, and for which the flexibility (and response to a compressive stress) can be tuned. A further improvement can consist in the use of external stimuli to modulate the mechanical properties of the materials enabling on-demand characteristics. Benzoxazine-based thermoresists are ideal candidates as their mechanical properties can be regulated through the subtle control of their curing process.[38,39] By incorporating an electrically conducting 2D material such as graphene in a polybenzoxazine thermoresist matrix, a conductive nanocomposite can be designed where the progressive polymerization of the resist, triggered by heating at specific temperatures, modulates the rigidity of the active material and, as a consequence, the piezoresistive response when pressure is applied.

Here, we describe a novel simple method for tuning the sensitivity of piezoresistive pressure sensors through *à la carte* modulation of the mechanical properties of the active material with temperature. We describe the generation of a novel graphene-based nanocomposite material assembled by combining chemically reduced graphene oxide (rGO) with a novel trifunctional polybenzoxazine thermoset precursor based on tris(3-aminopropyl)amine and phenol reagents (PtPA).[40] The resulting rGO-PtPA nanocomposite features combined properties of its individual components, i.e., the outstanding electrical properties of rGO and the adjustable mechanical properties of the PtPA thermoset resin. Flexible piezoresistive pressure sensors with programmed sensitivities ranging from 10^{-2} to 1 kPa^{-1} are fabricated. Furthermore, we demonstrate that the sensitivity of the pressure sensors can be readily modulated by controlling either the rGO:PtPA ratio or the rGO-PTPA curing temperature. Combined with solution processability compatible with large-area coatings technologies, and a thermal curing process compatible with most common commercial flexible substrates, our rGO-PtPA nanocomposite represents a proof-of-concept graphene-based nanocomposite formulation with on-demand tunable piezoresistive behavior, holding potential for commercial and industrial implementation in applications like pressure sensing for health monitoring and wearable electronics.

EXPERIMENTAL SECTION

Materials. Graphene oxide (GO) in aqueous dispersion (4 mg/mL) was purchased from Graphenea (Spain).

Ethanol (EtOH), isopropyl alcohol (IPA), sodium dithionite ($Na_2S_2O_4$), phenol (>99%), and ammonium hydroxide (NH_4OH) were purchased from Sigma-Aldrich Merck (France). Paraformaldehyde (>99%) and chloroform were purchased from VWR. All the reagents were used as supplied. ITO-covered PET substrates (ITO-PET, surface resistivity 60 Ω/sq., thickness of ITO coating: 130 nm) were purchased from Sigma-Aldrich Merck (France). Copper wire (0.35 mm diameter), polyimide (PI) tape (0.08 mm thickness), and silver paste were purchased from RS Components (France).

PtPA Synthesis and Characterization. Phenol/tris(3-aminopropyl)amine-based benzoxazine was synthesized as previously published.[40] Briefly, phenol (2.85 g, 0.03 mol), tris(3-aminopropyl)-amine (2 mL, 0.01 mol), and paraformaldehyde (1.82 g, 0.06 mol) were mixed in a 100 mL round-bottom flask, and 5 mL of chloroform was added per gram of reactants. The mixture was stirred at reflux for 4 h. After cooling to room temperature, the reaction mixture was added with anhydrous $MgSO_4$, filtered by Büchner, and dried under vacuum to obtain PtPA as a translucent soft solid. ^{1}H NMR ($CDCl_3$, ppm, δ): 7.24−6.65 (m, 12H, Ar), 4.84 (s, 6H, CH_2 oxazine), 3.96 (s, 6H, CH_2 oxazine), 2.79−2.70 (t, 6H, CH_2 propyl), 2.48−2.42 (t, 6H, CH_2 propyl), 1.71−1.63 (t, 6H, CH_2 propyl). FTIR ν (cm^{-1}): 1219 (asymmetric stretching of C−O−C), 1033 (symmetric stretching of C−O−C), 922 (benzene with an attached oxazine ring). For the Young modulus estimation by atomic force spectroscopy, force curves were collected using a Dimension Icon AFM (Bruker) equipped with RFESP-75 tips (spring constant 3 N/m, nominal radius 8 nm). A minimum of 25 force curves was collected for each sample in different locations.

rGO-PtPA Active Material Preparation and Characterization. Reduced graphene oxide (rGO) was obtained by chemical reduction of GO, following a procedure adapted from Karim et al.[41] Briefly, 110 mL of GO dispersion (i.e., 440 mg) was diluted with 330 mL of water and put at 90 °C on a hot plate. Then, 300 μL of NH_4OH and 3.3 g of $Na_2S_2O_4$ were added to the mixture. The reaction was carried out at 90 °C overnight, under continuous stirring. The final product consisted of a black solid, which was first decanted from the reaction mixture and then washed four times through centrifugation (9000 rpm, 30 min) with water (first washing step) and EtOH (further washing steps).

The obtained rGO was then dispersed in EtOH to a final stock concentration of 2 mg/mL.

The preparation of the rGO-PtPA active material was carried out by stirring overnight, at room temperature, aliquots of rGO dispersion mixed with appropriate quantities of PtPA solution (25 mg/mL in $CHCl_3$), to obtain rGO-PtPA composites with different rGO:thermoresist mass ratios. The blends were stored at 4 °C in stock solutions of 5 mg/mL. Aliquots of 1 mL were diluted 10-fold immediately before their use for film deposition through spray coating by means of an air brush (Timbertech ABPST01).

https://doi.org/10.1021/acs.chemmater.3c01191
Chem. Mater. 2023, 35, 6909−6919

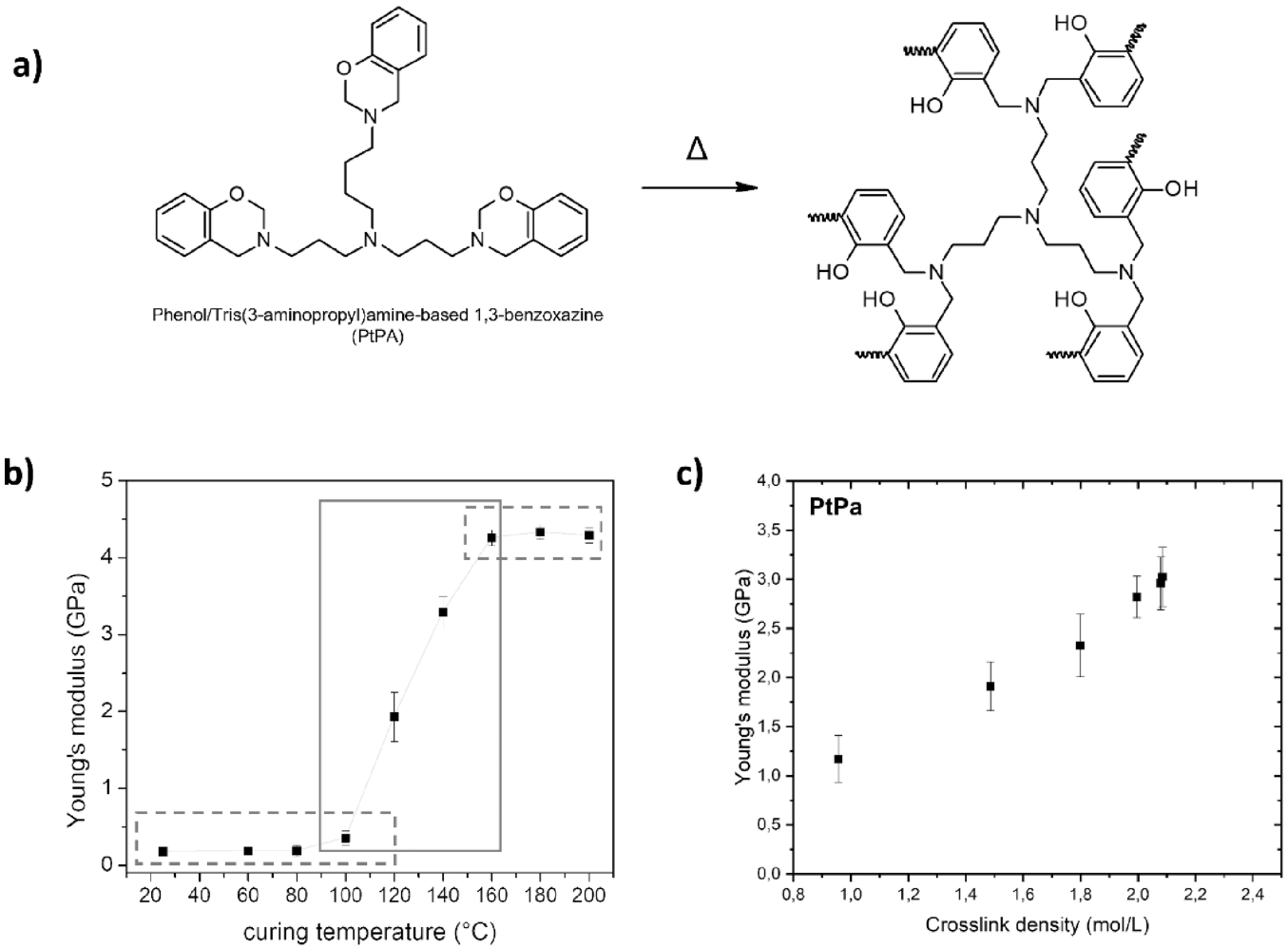

Figure 1. (a) Reaction scheme for PtPA curing reaction. (b) Young modulus of PtPA as a function of the curing temperature, as measured by atomic force spectroscopy. (c) Young's modulus of PtPA as a function of the crosslink density, as calculated using MD simulations.

The chemical composition of both rGO and rGO-PtPA active material was characterized through Fourier transform infrared spectroscopy (FTIR) and X-ray photoelectron spectroscopy (XPS).

The morphology and crystalline structures were studied with secondary electron microscopy (SEM) and X-ray diffraction (XRD).

For FTIR, XPS, and SEM analyses, rGO-PtPA active materials were deposited on SiO_2 substrates (1 cm^2 area). By spray coating 1 mL of rGO-PtPA stock solution at 80 °C, films with a 2.5 μm thickness were obtained, as assessed by stylus profilometry carried out with an Alpha-Step IQ profilometer (KLA-Tencor, USA), with a 500 μm scan length at a 50 μm/s scan rate.

FTIR spectra were collected in the range 4000−500 cm^{-1} (4 cm^{-1} resolution) using a FTIR-4700 Fourier transform infrared spectrometer (JASCO) equipped with a diamond crystal for attenuated total reflectance (ATR) measurements. XPS analysis was performed with a K-Alpha X-ray photoelectron spectrometer (Thermo Scientific, France) equipped with an Al K-alpha X-ray source and a hemispherical analyzer. Charge compensation was provided by a flood gun. For each sample, survey spectra were acquired as well as high-resolution spectra for C 1s, O 1s, and N 1s. SEM images were recorded with a FEI Quanta FEG 250 instrument S3 (FEI corporate, USA).

XRD analysis was carried out on sample powders, obtained by drying 2 mL of rGO-PtPA stock solution overnight at 60 °C. The spectra were collected with a D8 X-ray diffractometer (Bruker France SAS).

The electrical properties of the materials were characterized through four-point probe measurements and $I-V$ measurements as a function of temperature (range 80−300 K). For four-point probe analysis, 500 nm rGO-PtPA films were deposited by spray coating of 0.25 mL of stock solution on SiO_2; the measurements were carried out using a Jandel RM3000 instrument (Jandel Engineering Ltd., UK). For temperature-dependent electrical characterization, 500 nm films were spray coated onto interdigitated electrodes (IDE, MicruX, Spain) and $I-V$ characteristics as a function of temperature were collected between 80 and 300 K (20 K steps) by means of a liquid nitrogen-cooled cryostat (OptistatDN-V with ITC503S Cryogenic Temperature Controller, Oxford Instruments, UK) connected to the dual-channel Keithley 2636A Sourcemeter.

Modeling. For modeling, we used the Materials Studio 7.0 package to generate and construct the PtPA model systems. Initially, we placed 200 monomer molecules within 3D periodic cells at a relatively low density (0.6 g/cm^3). These structures underwent equilibration in the NVT ensemble at 500 K for 1 ns, succeeded by an NPT simulation at 300 K for 4 ns, leading to the formation of a dense phase. For the construction of the resin structures, we employed a previously established polymerization mechanism based on the cyclic polymerization atomistic model and multistep topology relaxation.[42,43] Elastic property calculations were performed using the LAMMPS package, by simultaneously applying longitudinal deformations and maintaining the NPT ensemble throughout the simulations. The optimized Dreiding force-field parameters from our preceding research were used in this study.[40] van der Waals and electrostatic interactions were reproduced using Lennard-Jones (12-6) and Coulombic potentials, respectively, within a predefined 1.2 nm cutoff distance. The atomic charges were calculated through the iterative

https://doi.org/10.1021/acs.chemmater.3c01191
Chem. Mater. 2023, 35, 6909−6919

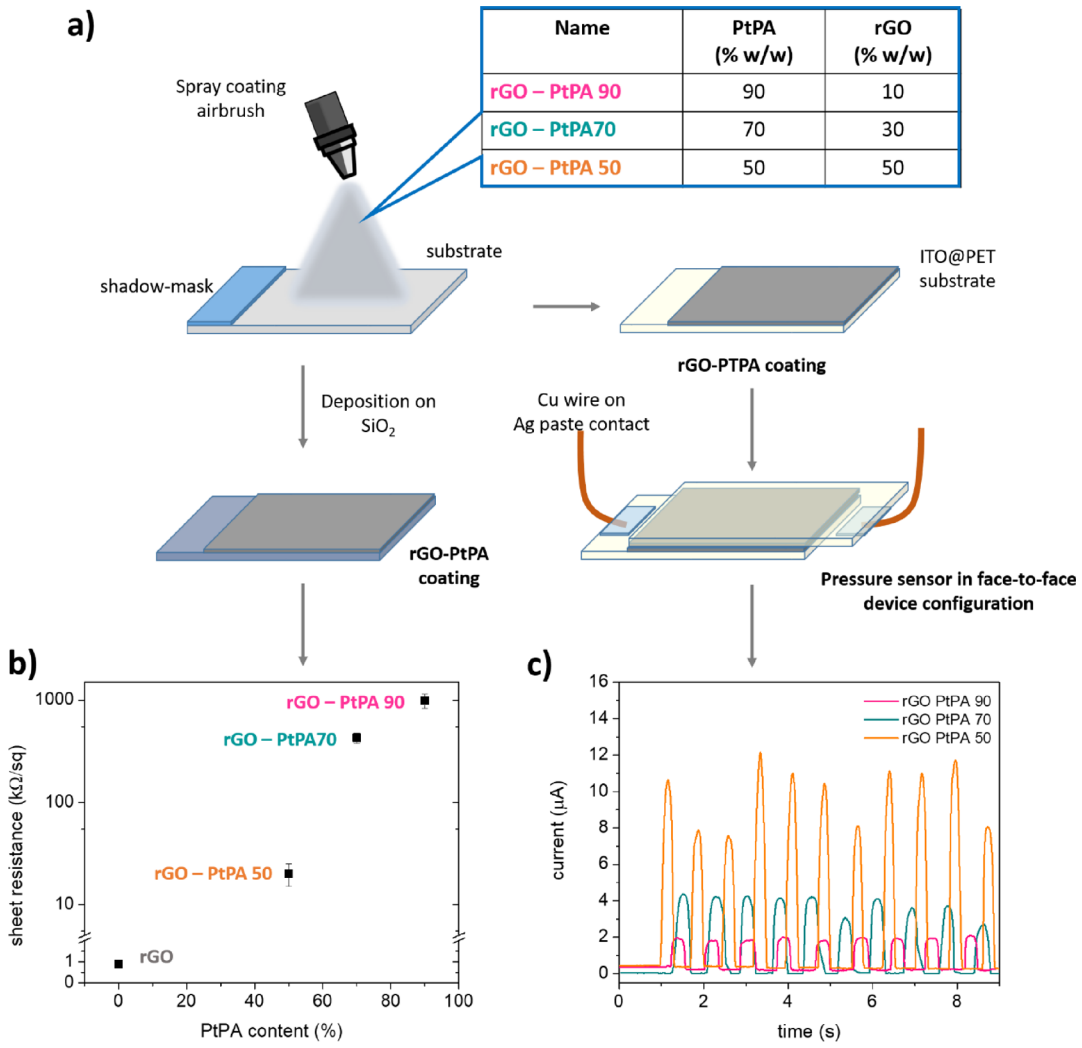

Figure 2. (a) Schematic of the spray-coating deposition of rGO-PtPA materials (whose compositions (%w/w)) are summarized in the inset table), for film characterization or assembly of flexible pressure sensors. (b) Sheet resistance (500 nm films) of the rGO-PtPA materials. (c) Plot of the current as a function of time measured for the pressure sensors (0.1 V bias) upon finger tapping on the device.

Gasteiger methodology. The NPT (constant number of particles, pressure, and temperature) simulations were performed maintaining a steady pressure with the Parrinello–Rahman barostat at 1 atm. The Nosé–Hoover–Langevin thermostat was used to regulate the system's temperature, a Q ratio of 0.01, and a decay constant of 1 ps.

Pressure Sensor Fabrication and Piezoresistive Performance Characterization. Graphene-based pressure sensing devices with tunable sensitivity were assembled as previously reported, with some modifications.[44] Briefly, the rGO-PtPA active material was spray coated at 80 °C onto rectangular chips of ITO-PET (13 mm × 20 mm). A shadow mask (13 mm × 5 mm) was applied prior to the spray coating, in order to leave part of the conductive substrate free of active material to place electrical contacts onto. The deposition of rGO-PtPA was monitored through UV–vis spectroscopy until a transmittance of 20% at 500 nm was achieved; such transmittance value was obtained after spraying 1 mL of dispersion per ITO-PET chip. After the active material deposition, the shadow mask was removed and two of the obtained electrodes were placed in a face-to-face configuration and fixed together using PI tape, in order to have a layer of active material sandwiched between two ITO-PET substrates. The devices were characterized and tested both as-prepared and after thermal curing at different temperatures (namely, 120 °C and 160 °C).

Electrical contacts were obtained on all the devices (as-prepared and annealed) by fixing copper wires with silver paste.

The devices' performance was evaluated in terms of pressure sensitivity and device durability upon application of cyclic stress. Such tests were carried out using a Mark-10 M7-025E digital force gauge mounted on a Mark-10 ESM-303E motorized test stand. The test setup was equipped with a round compression plate of 1.15 cm diameter.

The sensitivity was assessed through static pressure tests, consisting in the measurement of the device electrical resistivity when a static force was applied in the range 0.005 to 0.2 N (corresponding to a pressure range between 0.05 and 2 kPa). The resistivity was measured by means of a Keithley 2635B source meter.

Statistical Analysis. One-way analysis of variance (ANOVA) was used to evaluate statistical significance ($p < 0.05$). Error bars represent standard error of the mean, extrapolated from separate experiments on at least four different samples.

RESULTS AND DISCUSSION

Benzoxazine thermoresists constitute a class of phenolic resins characterized by excellent chemical stability and mechanical properties; examples are present in the literature of different polybenzoxazine-carbon nanomaterial composites, with perspective applications that include aerospace coatings, corrosion protection, electronics, and alloys.[45−47]

https://doi.org/10.1021/acs.chemmater.3c01191
Chem. Mater. 2023, 35, 6909−6919

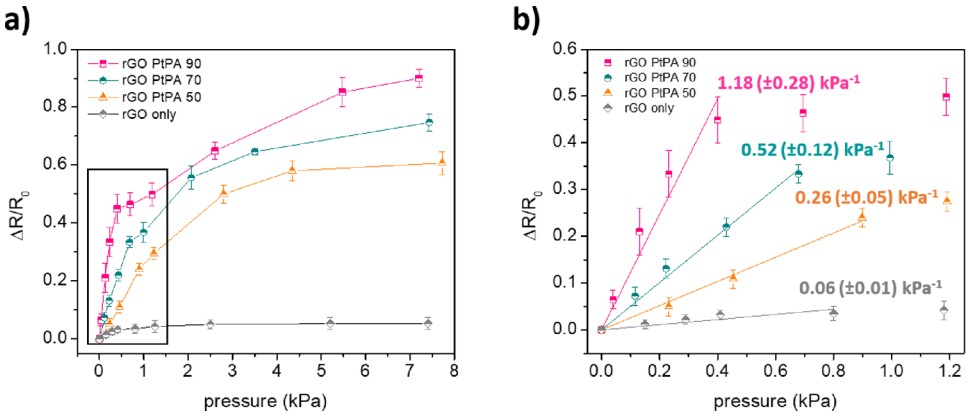

Figure 3. (a) Relative resistance as a function of the applied pressure for rGO-PtPA-based pressure sensors. (b) Detail of the relative resistance plot in the low-pressure regime; sensitivity of the various pressure sensors is indicated on the graph, as extrapolated from the linear fit of the relative resistance as a function of the pressure.

The polybenzoxazine, resulting from thermal curing of the PtPA precursor (Figure 1a), is an electrically insulating thermoset resin, whose degree of crosslinking can be tuned by controlling the time and temperature of curing. The elastic modulus (Young modulus) of PtPA thermoset resin can be expected to depend on the degree of crosslinking of the polymer.[48] This was confirmed by atomic force spectroscopy measurements, revealing a clear dependence of the magnitude of the elastic modulus on the curing temperature (Figure 1b). The modulus was found to increase linearly with the curing temperature between 100 and 160 °C, namely, from 0.18 to 4.30 GPa, respectively.

The modeling of PtPA structures allowed us to go beyond the experimental investigations by further investigating the connection between crosslink density and the Young's modulus as a function of crosslinking. By applying uniaxial deformation to simulated PtPA structures at different conversion degrees, with a maintained strain rate of 10^5 s^{-1}, we evaluated the strain−stress characteristics of the material. The linear elastic region identified during small deformations was used for the calculation of the Young's modulus at each individual conversion degree according to Hooke's law. The execution of these simulations across four independently prepared structures ensured the statistical reliability of our analysis, allowing for the determination of both average values and standard deviation. Figure 1c reveals that the calculated Young's modulus increases almost linearly with crosslink density before leveling off at around 3 GPa for full conversion. The computational predictions are in line with the experimental data and substantiate the close relationship between mechanical properties, as assessed by the Young's modulus, and the crosslinking degree (increasing with conversion rate). We note though that the simulated modulus at full conversion falls slightly short of the experimental value, a difference likely associated with inherent simplifications in our computational model. Nonetheless, these simulations present a valuable tool to deepen our understanding of the mechanical properties—3D structural organization relationships in polybenzoxazine thermoset resins.

Given the possibility of tuning the modulus (hence the rigidity) of the PtPA-based thermoset resin through an *ad hoc* curing treatment, we explored the possibility of developing pressure-sensitive active materials by combining reduced graphene oxide with PtPA resins.

Graphene-thermoresist active material was synthesized by mixing rGO dispersions (prepared by chemical reduction of GO)[41] with appropriate amounts of PtPA benzoxazine precursor solutions, yielding a homogeneous dispersion that can be processed and deposited as (thin) film onto a solid substrate. With the aim of tuning the contribution of the two components, namely, the modulable mechanical properties provided by the PtPA precursor and the electrical conductivity imparted by the rGO, three formulations were prepared and characterized, namely, rGO-PtPA 90, rGO-PtPA 70, and rGO-PtPA 50 comprising 10, 30, and 50% w/w rGO, respectively. Table S1 details the composition of each formulation in terms of mass content (%) of rGO and PtPA.

Preliminary assessments of the electrical properties were carried out in order to quantify the sheet resistance of rGO-PtPA films by means of four-point probe measurements on 500 nm-thick films of rGO-PtPA on SiO_2 substrates prepared by spray coating of 0.5 mg/mL dispersions in 1:1 chloroform−EtOH mixtures (Figure 2a). As anticipated, the measured sheet resistance was found to decrease from 990 to 20 kΩ/sq. with the increasing content of the conductive rGO component (Figure 2b and Table S1). For our system, a concentration of rGO below 10% w/w resulted in poor electrical properties, likely because the high concentration of benzoxazine did not allow for the formation of an effective conductive network between the rGO flakes dispersed in the precursor (according to percolation theory);[49,50] on the other hand, a concentration above 50% gave performances comparable with rGO alone, hence minimizing the contribution of PtPA in the blend.

To test the piezoresistive behavior of rGO-PtPA, pressure sensors were assembled by preparing two rGO-PtPA-coated electrodes and assembling them in a vertical junction in a face-to-face configuration (Figure 2a). Preliminary pressure sensing tests consisted in powering the sensors with a source meter (0.1 V bias) and measuring the current that is passing through the vertical device while repeatedly applying a light pressure (≈0.5 kPa) through finger-tapping. Figure 2c displays an increase in the measured current when pressure is applied, and the current increment increases when augmenting the content of rGO in the active material.

The sensitivity of the pressure sensors was systematically quantified by recording the relative resistance change (extrapolated from current measurements) as a function of the applied pressure (the latter provided by applying a known

https://doi.org/10.1021/acs.chemmater.3c01191
Chem. Mater. 2023, 35, 6909−6919

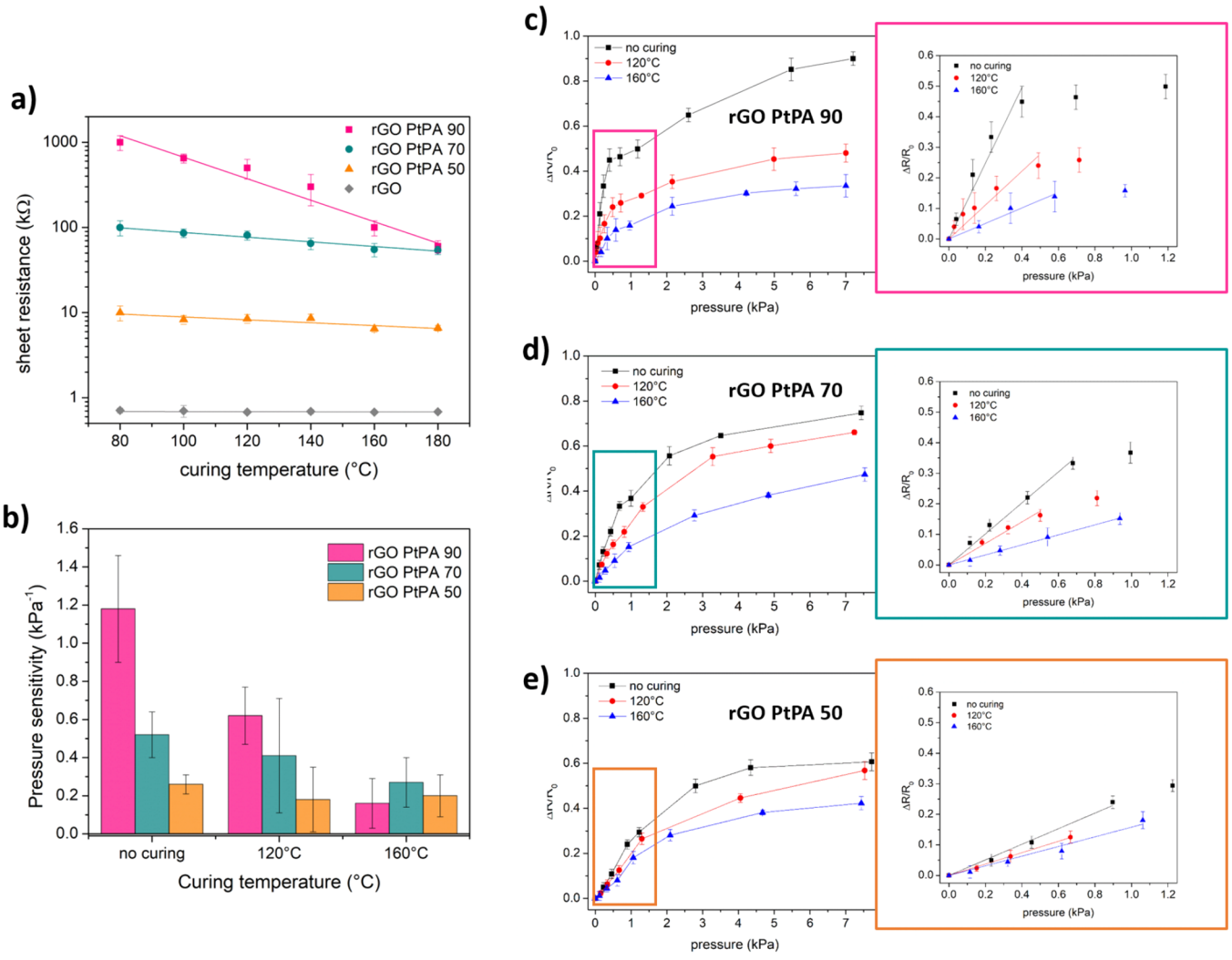

Figure 4. (a) Sheet resistance values (on 500 nm spray-coated films) of different rGO-PtPA materials after annealing at progressively higher temperatures. (b) Calculated pressure sensitivities of rGO-PtPA-based pressure sensors after different annealing treatments. The values are extrapolated from the linear fits of relative resistance measured as a function of the applied pressure, presented in (c), (d), and (e).

load with an automatized force gauge). The sensitivity was calculated from the plots of relative resistance as a function of the applied pressure following the equation:

$$S = \frac{(R_0 - R)}{R_0} P = \frac{\Delta R}{R_0} P$$

where R is the measured resistance when a load is applied, R_0 is the baseline resistance (unloaded), and P is the pressure arising from the applied load. In Figure 3, representative relative resistance plots are presented. From Figure 3a, we can clearly identify two pressure regimes: one where the largest variation in the relative resistance occurs (i.e., from 0 to 1 kPa) and one in which a very small variation of the relative resistance is observed while increasing the applied pressure (i.e., from about 2 to 7.5 kPa). To extrapolate the device sensitivity, the applied pressure range was selected between 0 and 1 kPa (Figure 3b), which is where the most significant variation occurs for the relative resistance. The second regime at pressure higher than 2 kPa is effectively outside the linearity range, with negligible response to the applied pressure (slope $\ll$ 0.0005 kPa^{-1}); hence, it was not taken into account for sensitivity calculation.

The highest sensitivity was achieved for the devices prepared with the rGO-PtPA active material with the larger content of PtPA (i.e., rGO-PtPA 90, with 1.18 kPa^{-1}); the sensitivity value was progressively lower as the resist content decreased in the formulation, namely, 0.52 kPa^{-1} for rGO-PtPA 70 and 0.26 kPa^{-1} for rGO-PtPA 50. These results provide evidence for the dependence of the pressure sensitivity of the active material on the amount of PtPA monomer precursor, consistent with a control of the material rigidity determined by the amount of "flexible" component (i.e., polymer precursor), considering rGO as the "rigid" element within the material. The pressure-sensitive behavior determined by the addition of PtPA is further confirmed by the considerably lower sensitivity achieved from sensors prepared using pristine rGO as active material, namely, 0.06 kPa^{-1} (i.e., one order of magnitude lower than the sensitivity of rGO-PtPA-based devices).

The pressure sensors prepared with rGO-PtPA active materials feature high sensitivity in the low-pressure regime, making them potentially exploitable for applications such as health monitoring or electronic skin. In terms of sensitivity, their performance is competitive with that of piezoresistive sensors based on several different microstructured or layered

https://doi.org/10.1021/acs.chemmater.3c01191
Chem. Mater. 2023, 35, 6909−6919

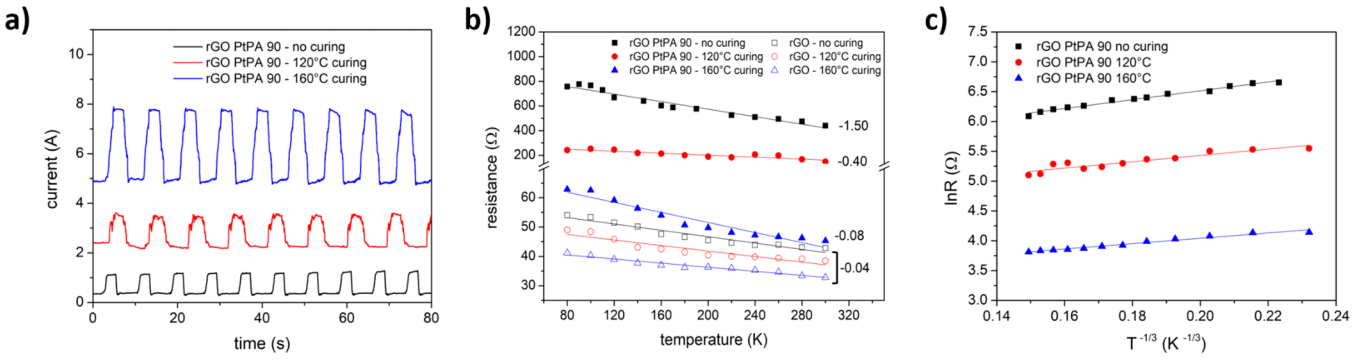

Figure 5. Functional, electrical, and structural characterization of the rGO PtPA 90 material at different stages of curing: (a) current measured upon cyclic application of a 0.5 kPa load on pressure sensors, (b) temperature-dependent electrical resistance (numbers represent the slope of the fitted line), (c) ln R vs $T^{-1/3}$ plots.

planar graphene-polymer systems as active sensing material (Table S2),[34,51] taking also into account the advantage of convenient material processing and device assembly, which requires neither harsh reaction conditions nor complex, time-consuming, and costly microfabrication methods.

The possibility of tuning the elastic modulus of PtPA through curing was explored in the context of rGO-PtPA active materials. For this purpose, pressure sensors prepared with different rGO-PtPA formulations were partially and completely cured upon exposure to 120 and 160 °C, respectively. The two temperatures were chosen to cover the whole range of the PtPA moduli values that can be achieved, as previously assessed by atomic force spectroscopy (Figure 1b). The adopted curing processes and temperatures are compatible with most common plastic substrates used in flexible electronics, including PET (Table S3); thus, the thermal stability of the sensor was ensured, preventing degradation upon thermal treatment.

The progressive crosslinking of PtPA monomer at different curing temperatures was confirmed through FTIR spectroscopy; on the spectra (Figure S1), we can observe an intensity decrease of the bands at 1033 cm^{-1} (C−O−C symmetric stretching), 1220 cm^{-1} (C−O−C asymmetric stretching), and 922 cm^{-1} (characteristic of a phenyl ring with an attached oxazine ring), which completely disappear when the crosslinking process is complete at 160 °C.[52]

The rGO-PtPA material structure and morphology upon curing were also characterized by SEM and XRD. From SEM images of the films (Figure S2) no difference is observed on the surface morphology of the samples as a consequence of the curing treatment. The XRD patterns for the rGO-PtPA materials (Figure S3) are characterized by a broad peak at diffraction angles between 12 and 30°, which shifts toward higher diffraction angles as the rGO-PtPA ratio in the formulation increases, going from 18.4 to 22.1 and 23.7°, for rGO-PtPA 90, rGO-PtPA 70, and rGO-PtPA 50, respectively.

This peak could be assigned either to the 002 graphitic plane reflection, characteristic of the graphene-related component of the material,[53] or to a broad reflection arising from the amorphous PtPA monomer and crosslinked.[54] In both cases, the peak maximum shifting toward lower diffraction angles (i.e., larger interlayer distances) upon increase of PtPA content in the composite is consistent with either intercalation of benzoxazine within the rGO sheets (thus the increase of the interlayer distance) or a masking effect of PtPA over the reflection of the 002 graphitic plane. However, for all the three formulations, no structural change is observed after annealing. For instance, no shift or significant change in FWHM is shown for the main peak after the different curing treatments. Combined with the constant presence of a peak at 42.8°, related to 100 graphitic plane reflection[55,56] in all the samples, the data discussed above indicate that no aggregation is induced on the graphene backbone by thermal annealing. Hence, we can speculate that the polybenzoxazine is effectively well incorporated within the rGO sheets.

The pressure sensitivity of the devices was then assessed as described above, and the results are reported in Figure 4. A general decrease of the sensitivity is observed, with a significant variation being obtained for the devices prepared with the rGO-PtPA 90 active material. This behavior is consistent with the contribution of the PtPA component that becomes more rigid upon curing; such contribution is greater for the formulation containing a larger amount of thermoresist precursor, which then undergoes crosslinking to result in a progressively more rigid resin. The consequent decrease in the active material rigidity is consistent with the lower pressure sensitivity. The contribution of PtPA curing degree to the material rigidity is lower or negligible when the concentration of monomer precursor is lower.

The results presented demonstrate that for the obtained graphene-PtPA benzoxazine materials, a modulation of the pressure sensitivity can be achieved via the *ad hoc* selection of the rGO:PtPA ratio. Most importantly, among the prepared graphene-benzoxazine formulations, rGO PtPA 90 shows promise in terms of on-demand tuning of the sensitivity by means of an external stimulus (in this case, heat); within a single material, it was possible to modulate the sensitivity to cover the range 10^{-2}−1 kPa^{-1} in the low-pressure regime. Such modulation of the pressure sensitivity of a graphene-based material was previously achieved through cumbersome approaches consisting in preparing separate systems having either different chemical functionalization of the graphene skeleton or microstructures with different geometries (or varying density of the same geometrical features).[35,44,57−59]

To understand the different piezoresistive behavior shown by rGO PtPA 90 upon curing, further characterization was carried out to study the material electrical properties. Together with a decrease of the pressure responsiveness upon curing (i.e., decreased sensitivity), an increase in the baseline current in the absence of external pressure applied can be observed for rGO PtPA 90 (Figure 5a). This is consistent with the decrease in the sheet resistance measured by four-point probe technique

https://doi.org/10.1021/acs.chemmater.3c01191
Chem. Mater. 2023, 35, 6909−6919

when no load is applied (Figure 4a). Such a trend in the sheet resistance decrease upon curing was observed for all the three rGO-PtPA formulations, but the most striking variation was seen in rGO PtPA 90.

The changes in the electrical properties of rGO PtPA 90 upon curing were studied by carrying out temperature-dependent measurements on films deposited onto interdigitated gold electrodes. A significant decrease in the electrical resistance is observed for the as-deposited (non-cured) film when the temperature increases (Figure 5b). Interestingly, this temperature dependence progressively decreases when the material is annealed, paired with a one-order of magnitude decrease in the electrical resistance.

The dependence of the resistance on the measurement temperature supports an activated electrical transport process, and in the case of insulator−conductor nanocomposites (including those based on graphene and reduced graphene oxide), this process is usually well described by a hopping mechanism, where the charge transport occurs mainly via hopping through available localized states.[60] Hopping can be described by the following general equation:[61,62]

$$R(T) = R_0 e^{\left(\frac{T_0}{T}\right)^p}$$

where R is the resistivity, T is the temperature at which R is measured, R_0 and T_0 are constants, and p is an exponential factor. The latter depends on the specific hopping mechanism occurring in the material, and it is defined as

$$p = \frac{1}{(D+1)}$$

with D being the dimensionality of the system. In particular, the exponent p results to be 1/3 for 2D Mott variable-range hopping (VRH), 1/4 for 3D Mott VRH, 1/2 for 2D Efros−Shklovskii VRH, or 1 for the thermally activated Arrhenius-like transport mechanism (corresponding to nearest neighborhood hopping (NNH).[60,63] Extensive treatment of the different models and mathematical and physical descriptions are out of the scope of this work and can be found elsewhere.

In our case, the experimental data were best fitted (i.e., $R^2 > 0.9$) when plotting $\ln(R)$ vs $T^{-1/3}$, thus supporting a 2D Mott VRH mechanism. The dimensionality of the system $D = 2$ (which results in $p = 1/3$) is also consistent with the layered structure of the rGO-PtPA material in which the electrical transport most likely happens in two dimensions. The linear dependence of ln R as a function of $T^{-1/3}$ for the non-cured and cured films confirms a Mott VRH conduction mechanism (Figure 5c). This type of electrical behavior is often observed for insulating polymers loaded with conductive fillers, the latter creating a conductive/percolative network within the insulating matrix.[50] Also, this conduction mechanism has been reported for hybrid systems featuring layered polymer-rGO structures similar to the one of rGO PtPA 90.[64,65]

Despite the analogous conduction mechanism for the material at different curing stages, the decrease in the temperature dependence of the resistivity upon curing (shown by the decrease of the slopes in the R vs T plots, Figure 5b) as well as the increase in the material conductivity (Figure 4a) indicate that a transition toward a metallic behavior is taking place when the material is being annealed;[66] specifically, the temperature-dependent electrical behavior of rGO PtPA 90 upon curing progressively approaches the behavior of rGO alone. On the other hand, rGO alone does not show any temperature-dependent resistivity changes upon annealing treatments in the same conditions as for rGO PtPA 90. The slight change in the value of the resistivity can be ascribed to an improvement of the electrode−rGO interface upon annealing, which is independent from the rGO electrical characteristics.[67,68] This data, combined with no changes in C/O ratios (as measured by XPS, Figure S4 and Table S2) nor in sheet resistance (measured by a four-point probe, Figure 4a), rules out that the improvement in rGO PtPA 90 electrical characteristics is caused by further reduction of the rGO component, which does not take place upon thermal treatment in the conditions used for rGO-PtPA materials.

Excluding a contribution of the annealing of the rGO in the change of electrical properties of the composite, including the pressure response behavior, means that the crosslinking of the polybenzoxazine matrix dominates. It is well established that when a strain is applied on a graphene-polymer composite, a rearrangement of the microstructure of the conductive nanomaterial network takes place, which directly affects the electrical properties through variations in the overlap between the conductive sheets as well as the creation of new percolative paths.[50,69] Despite that the crosslinked and rigid PtPA polybenzoxazine is *per se* electrically insulating, the progressive crosslinking of the polymer could lead to a rearrangement in the graphene skeleton that increases the rGO sheets overlap or creates new percolative paths (or both). The same type of rearrangement should take place when a load is applied on the material film, and this theory is consistent with the combination of increased conductivity and decreased sensitivity for the cured rGO PtPA 90. A schematic of this process is portrayed in Figure 6.

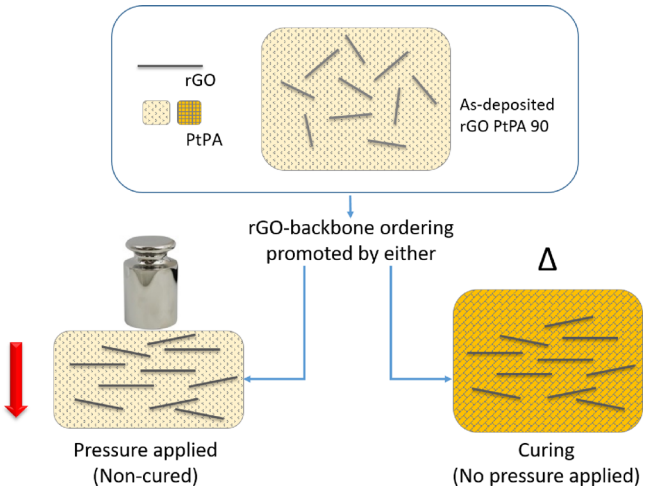

Figure 6. Schematics of the rGO rearrangement responsible for the increase in the rGO PtPA 90 conductivity; an analogous result could be achieved either through thermal curing or by applying a pressure load on the as-prepared material.

CONCLUSIONS

We reported the formulation of a novel nanocomposite material with tunable piezoresistive behavior, based on the integration of rGO with PtPA polybenzoxazine thermoset resin (rGO-PtPA). By combining the outstanding electrical properties of rGO with the tunable mechanical properties of the PtPA resin, rGO-PtPA materials have been prepared in different formulations and tested as active materials for pressure sensing

https://doi.org/10.1021/acs.chemmater.3c01191
Chem. Mater. 2023, 35, 6909−6919

applications. Flexible pressure sensors were fabricated, and it was shown that their sensitivity can be modulated by controlling either the rGO-PtPA ratio or the curing temperature. Modulation of the sensitivity from 10^{-2} to 1 kPa^{-1} is achieved in the low-pressure regime (up to 1 kPa) within a single material formulation. Our rGO-PtPA materials represent a proof-of-concept graphene-based material with on-demand piezoresponsive behavior that can be finely tuned through appropriate annealing treatments. Considering the material solution processability, compatibility with large-area coatings deposition, and the thermal curing process at mild temperature, i.e., compatible with most common commercial flexible substrates, rGO-PtPA composites offer great potential for commercial and industrial implementation in applications such as pressure sensing for health monitoring and wearable electronics.

■ ASSOCIATED CONTENT

Supporting Information

The Supporting Information is available free of charge at https://pubs.acs.org/doi/10.1021/acs.chemmater.3c01191.

FTIR spectra, powder XRD, SEM micrographs, and XPS spectra for representative rGO PtPA materials at different curing stages, with rGO analysis reported as reference; rGO PtPA material composition and measured sheet resistance; sensitivity for graphene-based pressure sensors prepared using different experimental methods and thermal properties of conventional polymeric substrates used for flexible electronics applications (PDF)

■ AUTHOR INFORMATION

Corresponding Authors

Artur Ciesielski − *Université de Strasbourg, CNRS, ISIS, Strasbourg 67000, France;* orcid.org/0000-0003-3542-4092; Email: ciesielski@unistra.fr

David Beljonne − *Laboratory for Chemistry of Novel Materials, Center of Innovation and Research in Materials & Polymers (CIRMAP-Materia Nova), Materials Research Institute, University of Mons (UMONS), B-7000 Mons, Belgium;* orcid.org/0000-0002-2989-3557; Email: david.beljonne@umons.ac.be

Paolo Samorì − *Université de Strasbourg, CNRS, ISIS, Strasbourg 67000, France;* orcid.org/0000-0001-6256-8281; Email: samori@unistra.fr

Authors

Stefania Vitale − *Université de Strasbourg, CNRS, ISIS, Strasbourg 67000, France;* orcid.org/0000-0002-7039-9470

Hugo Puozzo − *Laboratory for Chemistry of Novel Materials, Center of Innovation and Research in Materials & Polymers (CIRMAP-Materia Nova), Materials Research Institute and Laboratory of Polymeric and Composite Materials (LPCM), Center of Innovation and Research in Materials & Polymers (CIRMAP-Materia Nova), Materials Research Institute, University of Mons (UMONS), B-7000 Mons, Belgium;* orcid.org/0000-0002-0700-8449

Shamil Saiev − *Laboratory for Chemistry of Novel Materials, Center of Innovation and Research in Materials & Polymers (CIRMAP-Materia Nova), Materials Research Institute, University of Mons (UMONS), B-7000 Mons, Belgium*

Leïla Bonnaud − *Laboratory of Polymeric and Composite Materials (LPCM), Center of Innovation and Research in Materials & Polymers (CIRMAP-Materia Nova), Materials Research Institute, University of Mons (UMONS), B-7000 Mons, Belgium*

Antonio Gaetano Ricciardulli − *Université de Strasbourg, CNRS, ISIS, Strasbourg 67000, France;* orcid.org/0000-0003-2688-9912

Complete contact information is available at: https://pubs.acs.org/10.1021/acs.chemmater.3c01191

Author Contributions

The manuscript was written through contributions of all authors. All authors have given approval to the final version of the manuscript and declare no conflict of interest.

Notes

The authors declare no competing financial interest.

■ ACKNOWLEDGMENTS

This work was supported by the PROSPECT project funded by the FLAG-ERA programme (ANR-19-GRF1-0005-02), the EC through the ERC project SUPRA2DMAT (GA-833707), and the Graphene Flagship Core 3 project (GA-881603) as well as the Agence Nationale de la Recherche through the Interdisciplinary Thematic Institute SysChem via the IdEx Unistra (ANR-10-IDEX-0002) within the program Investissement d'Avenir, the International Center for Frontier Research in Chemistry (icFRC), and the Institut Universitaire de France (IUF). D.B. is an FNRS Research Director.

■ REFERENCES

(1) Khan, Y.; Ostfeld, A. E.; Lochner, C. M.; Pierre, A.; Arias, A. C. Monitoring of Vital Signs with Flexible and Wearable Medical Devices. *Adv. Mater.* **2016**, *28*, 4373−4395.

(2) Ma, Y.; Zhang, Y.; Cai, S.; Han, Z.; Liu, X.; Wang, F.; Cao, Y.; Wang, Z.; Li, H.; Chen, Y.; Feng, X. Flexible Hybrid Electronics for Digital Healthcare. *Adv. Mater.* **2020**, *32*, No. 1902062.

(3) Li, X.; Dunn, J.; Salins, D.; Zhou, G.; Zhou, W.; Schüssler-Fiorenza Rose, S. M.; Perelman, D.; Colbert, E.; Runge, R.; Rego, S.; Sonecha, R.; Datta, S.; McLaughlin, T.; Snyder, M. P. Digital Health: Tracking Physiomes and Activity Using Wearable Biosensors Reveals Useful Health-Related Information. *PLoS Biol.* **2017**, *15*, No. e2001402.

(4) Chen, T.; Shi, Q.; Zhu, M.; He, T.; Sun, L.; Yang, L.; Lee, C. Triboelectric Self-Powered Wearable Flexible Patch as 3D Motion Control Interface for Robotic Manipulator. *ACS Nano* **2018**, *12*, 11561−11571.

(5) Tee, B. C. K.; Wang, C.; Allen, R.; Bao, Z. An electrically and mechanically self-healing composite with pressure- and flexion-sensitive properties for electronic skin applications. *Nat. Nanotechnol.* **2012**, *7*, 825−832.

(6) Yang, J. C.; Mun, J.; Kwon, S. Y.; Park, S.; Bao, Z.; Park, S. Electronic Skin: Recent Progress and Future Prospects for Skin-Attachable Devices for Health Monitoring, Robotics, and Prosthetics. *Adv. Mater.* **2019**, *31*, No. 1904765.

(7) Mehrdad, S.; Wang, Y.; Atashzar, S. F. Perspective: Wearable Internet of Medical Things for Remote Tracking of Symptoms, Prediction of Health Anomalies, Implementation of Preventative Measures, and Control of Virus Spread During the Era of COVID-19. *Front. Rob. AI* **2021**, *8*, No. 610653.

(8) Singh, K. R. B.; Nayak, V.; Singh, J.; Singh, R. P. Nano-enabled wearable sensors for the Internet of Things (IoT). *Mater. Lett.* **2021**, *304*, No. 130614.

(9) Zang, Y.; Zhang, F.; Di, C.-a.; Zhu, D. Advances of flexible pressure sensors toward artificial intelligence and health care applications. *Mater. Horiz.* **2015**, *2*, 140−156.
(10) Choi, S.; Lee, H.; Ghaffari, R.; Hyeon, T.; Kim, D.-H. Recent Advances in Flexible and Stretchable Bio-Electronic Devices Integrated with Nanomaterials. *Adv. Mater.* **2016**, *28*, 4203−4218.
(11) Biccai, S.; Boland, C. S.; O'Driscoll, D. P.; Harvey, A.; Gabbett, C.; O'Suilleabhain, D. R.; Griffin, A. J.; Li, Z.; Young, R. J.; Coleman, J. N. Negative Gauge Factor Piezoresistive Composites Based on Polymers Filled with MoS_2 Nanosheets. *ACS Nano* **2019**, *13*, 6845−6855.
(12) Yang, N.; Liu, H.; Yin, X.; Wang, F.; Yan, X.; Zhang, X.; Cheng, T. Flexible Pressure Sensor Decorated with MXene and Reduced Graphene Oxide Composites for Motion Detection, Information Transmission, and Pressure Sensing Performance. *ACS Appl. Mater. Interfaces* **2022**, *14*, 45978−45987.
(13) Segev-Bar, M.; Landman, A.; Nir-Shapira, M.; Shuster, G.; Haick, H. Tunable Touch Sensor and Combined Sensing Platform: Toward Nanoparticle-based Electronic Skin. *ACS Appl. Mater. Interfaces* **2013**, *5*, 5531−5541.
(14) Jayathilaka, W. A. D. M.; Qi, K.; Qin, Y.; Chinnappan, A.; Serrano-García, W.; Baskar, C.; Wang, H.; He, J.; Cui, S.; Thomas, S. W.; Ramakrishna, S. Significance of Nanomaterials in Wearables: A Review on Wearable Actuators and Sensors. *Adv. Mater.* **2019**, *31*, 1805921.
(15) Chiappim, W.; Fraga, M. A.; Furlan, H.; Ardiles, D. C.; Pessoa, R. S. The status and perspectives of nanostructured materials and fabrication processes for wearable piezoresistive sensors. *Microsyst. Technol.* **2022**, *28*, 1561−1580.
(16) Zheng, Q.; Lee, J.-H.; Shen, X.; Chen, X.; Kim, J.-K. Graphene-based wearable piezoresistive physical sensors. *Mater. Today* **2020**, *36*, 158−179.
(17) Boland, C. S.; Khan, U.; Backes, C.; O'Neill, A.; McCauley, J.; Duane, S.; Shanker, R.; Liu, Y.; Jurewicz, I.; Dalton, A. B.; Coleman, J. N. Sensitive, High-Strain, High-Rate Bodily Motion Sensors Based on Graphene−Rubber Composites. *ACS Nano* **2014**, *8*, 8819−8830.
(18) Boland, C. S.; Khan, U.; Ryan, G.; Barwich, S.; Charifou, R.; Harvey, A.; Backes, C.; Li, Z.; Ferreira, M. S.; Möbius, M. E.; Young, R. J.; Coleman, J. N. Sensitive electromechanical sensors using viscoelastic graphene-polymer nanocomposites. *Science* **2016**, *354*, 1257−1260.
(19) Ren, H.; Zheng, L.; Wang, G.; Gao, X.; Tan, Z.; Shan, J.; Cui, L.; Li, K.; Jian, M.; Zhu, L.; Zhang, Y.; Peng, H.; Wei, D.; Liu, Z. Transfer-Medium-Free Nanofiber-Reinforced Graphene Film and Applications in Wearable Transparent Pressure Sensors. *ACS Nano* **2019**, *13*, 5541−5548.
(20) Cao, M.; Wang, M.; Li, L.; Qiu, H.; Padhiar, M. A.; Yang, Z. Wearable rGO-Ag NW@cotton fiber piezoresistive sensor based on the fast charge transport channel provided by Ag nanowire. *Nano Energy* **2018**, *50*, 528−535.
(21) Zhang, L.; Li, H.; Lai, X.; Gao, T.; Yang, J.; Zeng, X. Thiolated Graphene@Polyester Fabric-Based Multilayer Piezoresistive Pressure Sensors for Detecting Human Motion. *ACS Appl. Mater. Interfaces* **2018**, *10*, 41784−41792.
(22) Zhao, Y.; Liu, L.; Li, Z.; Wang, F.; Chen, X.; Liu, J.; Song, C.; Yao, J. Facile fabrication of highly sensitive and durable cotton fabric-based pressure sensors for motion and pulse monitoring. *J. Mater. Chem. C* **2021**, *9*, 12605−12614.
(23) Zhu, B.; Niu, Z.; Wang, H.; Leow, W. R.; Wang, H.; Li, Y.; Zheng, L.; Wei, J.; Huo, F.; Chen, X. Microstructured Graphene Arrays for Highly Sensitive Flexible Tactile Sensors. *Small* **2014**, *10*, 3625−3631.
(24) Yang, J.; Ye, Y.; Li, X.; Lü, X.; Chen, R. Flexible, conductive, and highly pressure-sensitive graphene-polyimide foam for pressure sensor application. *Compos. Sci. Technol.* **2018**, *164*, 187−194.
(25) Berger, C.; Phillips, R.; Centeno, A.; Zurutuza, A.; Vijayaraghavan, A. Capacitive pressure sensing with suspended graphene−polymer heterostructure membranes. *Nanoscale* **2017**, *9*, 17439−17449.
(26) Šiškins, M.; Lee, M.; Wehenkel, D.; van Rijn, R.; de Jong, T. W.; Renshof, J. R.; Hopman, B. C.; Peters, W. S. J. M.; Davidovikj, D.; van der Zant, H. S. J.; Steeneken, P. G. Sensitive capacitive pressure sensors based on graphene membrane arrays. *Microsyst. Nanoeng.* **2020**, *6*, 102.
(27) Chen, Z.; Wang, Z.; Li, X.; Lin, Y.; Luo, N.; Long, M.; Zhao, N.; Xu, J.-B. Flexible Piezoelectric-Induced Pressure Sensors for Static Measurements Based on Nanowires/Graphene Heterostructures. *ACS Nano* **2017**, *11*, 4507−4513.
(28) Mohammed, M. K.; Al-Nafiey, A.; Al-Dahash, G. Manufacturing Graphene and Graphene-based Nanocomposite for Piezoelectric Pressure Sensor Application: A Review. *Nano Biomed. Eng.* **2021**, *13*, 27−35.
(29) He, J.; Zhang, Y.; Zhou, R.; Meng, L.; Chen, T.; Mai, W.; Pan, C. Recent advances of wearable and flexible piezoresistivity pressure sensor devices and its future prospects. *J. Materiomics* **2020**, *6*, 86−101.
(30) Yao, H.-B.; Ge, J.; Wang, C.-F.; Wang, X.; Hu, W.; Zheng, Z.-J.; Ni, Y.; Yu, S.-H. A Flexible and Highly Pressure-Sensitive Graphene−Polyurethane Sponge Based on Fractured Microstructure Design. *Adv. Mater.* **2013**, *25*, 6692−6698.
(31) Choong, C.-L.; Shim, M.-B.; Lee, B.-S.; Jeon, S.; Ko, D.-S.; Kang, T.-H.; Bae, J.; Lee, S. H.; Byun, K.-E.; Im, J.; Jeong, Y. J.; Park, C. E.; Park, J.-J.; Chung, U.-I. Highly Stretchable Resistive Pressure Sensors Using a Conductive Elastomeric Composite on a Micropyramid Array. *Adv. Mater.* **2014**, *26*, 3451−3458.
(32) Su, B.; Gong, S.; Ma, Z.; Yap, L. W.; Cheng, W. Mimosa-Inspired Design of a Flexible Pressure Sensor with Touch Sensitivity. *Small* **2015**, *11*, 1886−1891.
(33) Ma, C.; Xu, D.; Huang, Y.-C.; Wang, P.; Huang, J.; Zhou, J.; Liu, W.; Li, S.-T.; Huang, Y.; Duan, X. Robust Flexible Pressure Sensors Made from Conductive Micropyramids for Manipulation Tasks. *ACS Nano* **2020**, *14*, 12866−12876.
(34) Cao, M.; Su, J.; Fan, S.; Qiu, H.; Su, D.; Li, L. Wearable piezoresistive pressure sensors based on 3D graphene. *Chem. Eng. J.* **2021**, *406*, No. 126777.
(35) Park, J.; Lee, Y.; Hong, J.; Ha, M.; Jung, Y.-D.; Lim, H.; Kim, S. Y.; Ko, H. Giant Tunneling Piezoresistance of Composite Elastomers with Interlocked Microdome Arrays for Ultrasensitive and Multimodal Electronic Skins. *ACS Nano* **2014**, *8*, 4689−4697.
(36) Li, Z.; Li, B.; Chen, B.; Zhang, J.; Li, Y. 3D printed graphene/polyurethane wearable pressure sensor for motion fitness monitoring. *Nanotechnology* **2021**, *32*, No. 395503.
(37) Huang, C.-B.; Ciesielski, A.; Samorì, P. Molecular Springs: Integration of Complex Dynamic Architectures into Functional Devices. *Angew. Chem., Int. Ed.* **2020**, *59*, 7319−7330.
(38) Kiskan, B.; Yagci, Y. Benzoxazine resins as smart materials and future perspectives. In *Thermosets*; 2nd ed.; Guo, Q., Ed.; Elsevier, 2018; pp. 543−576.
(39) Santhosh Kumar, K. S.; Reghunadhan Nair, C. P.; Ninan, K. N. Rheokinetic investigations on the thermal polymerization of benzoxazine monomer. *Thermochim. Acta* **2006**, *441*, 150−155.
(40) Puozzo, H.; Saiev, S.; Bonnaud, L.; De Winter, J.; Lazzaroni, R.; Beljonne, D. Robust and Direct Route for the Development of Elastomeric Benzoxazine Resins by Copolymerization with Amines. *Macromolecules* **2022**, *55*, 10831−10841.
(41) Karim, N.; Afroj, S.; Tan, S.; He, P.; Fernando, A.; Carr, C.; Novoselov, K. S. Scalable Production of Graphene-Based Wearable E-Textiles. *ACS Nano* **2017**, *11*, 12266−12275.
(42) Saiev, S.; Bonnaud, L.; Dumas, L.; Zhang, T.; Dubois, P.; Beljonne, D.; Lazzaroni, R. Do Carbon Nanotubes Improve the Thermomechanical Properties of Benzoxazine Thermosets? *ACS Appl. Mater. Interfaces* **2018**, *10*, 26669−26677.
(43) Saiev, S.; Bonnaud, L.; Zúñiga, C.; Dubois, P.; Beljonne, D.; Ronda, J. C.; Cadiz, V.; Lazzaroni, R. Positive effect of functional side groups on the structure and properties of benzoxazine networks and nanocomposites. *Polym. Chem.* **2019**, *10*, 5251−5264.
(44) Huang, C.-B.; Witomska, S.; Aliprandi, A.; Stoeckel, M.-A.; Bonini, M.; Ciesielski, A.; Samorì, P. Molecule-Graphene Hybrid

Materials with Tunable Mechanoresponse: Highly Sensitive Pressure Sensors for Health Monitoring. *Adv. Mater.* **2019**, *31*, No. 1804600.
(45) Wang, T.; Quinn, M. D. J.; Nguyen, S. H. T.; Yu, A.; Notley, S. M. Graphene Films Using a Thermally Curable Surfactant. *Adv. Mater. Interfaces* **2016**, *3*, No. 1600182.
(46) Biru, I.; Damian, C. M.; Gârea, S. A.; Iovu, H. Benzoxazine-functionalized graphene oxide for synthesis of new nanocomposites. *Eur. Polym. J.* **2016**, *83*, 244−255.
(47) Bîru, E. I.; Gârea, S. A.; Iovu, H. Developing Polybenzoxazine Composites Based on Various Carbon Structures. *Macromol. Chem. Phys.* **2019**, *220*, No. 1800322.
(48) Tsygankov, S. A.; Gol'dman, A. Y. Changes in the elastic modulus of thermosetting polymers during curing. *Polym. Sci. U.S.S.R.* **1979**, *21*, 321−326.
(49) Essam, J. W. Percolation Theory. *Rep. Prog. Phys.* **1980**, *43*, 833−912.
(50) Marsden, A. J.; Papageorgiou, D. G.; Vallés, C.; Liscio, A.; Palermo, V.; Bissett, M. A.; Young, R. J.; Kinloch, I. A. Electrical percolation in graphene-polymer composites. *2D Mater.* **2018**, *5*, No. 032003.
(51) Cui, X.; Huang, F.; Zhang, X.; Song, P.; Zheng, H.; Chevali, V.; Wang, H.; Xu, Z. Flexible pressure sensors via engineering microstructures for wearable human-machine interaction and health monitoring applications. *iScience* **2022**, *25*, No. 104148.
(52) Gârea, S.-A.; Iovu, H.; Nicolescu, A.; Deleanu, C. Thermal polymerization of benzoxazine monomers followed by GPC, FTIR and DETA. *Polym. Test.* **2007**, *26*, 162−171.
(53) Kakaei, K.; Esrafili, M. D.; Ehsani, A., Characterization. In *Iterface Science and Technology*; Kakaei, K.; Esrafili, M. D.; Ehsani, A., Eds.; Elsevier, 2019; Vol. *27*, pp. 109−151.
(54) Kumar, R. S.; Ariraman, M.; Alagar, M. Studies on dielectric properties of GO reinforced bisphenol-Z polybenzoxazine hybrids. *RSC Adv.* **2015**, *5*, 23787−23797.
(55) Boukhoubza, I.; Khenfouch, M.; Achehboune, M.; Mothudi, B. M.; Zorkani, I.; Jorio, A. X-ray diffraction investigations of nanostructured ZnO coated with reduced graphene oxide. *J. Phys.: Conf. Ser.* **2019**, *1292*, No. 012011.
(56) Li, H.; Sun, L.; Zhang, Y.; Tan, T.; Wang, G.; Bakenov, Z. Enhanced cycle performance of Li/S battery with the reduced graphene oxide/activated carbon functional interlayer. *J. Energy Chem.* **2017**, *26*, 1276−1281.
(57) Park, J.; Lee, Y.; Lim, S.; Lee, Y.; Jung, Y.; Lim, H.; Ko, H. Ultrasensitive Piezoresistive Pressure Sensors Based on Interlocked Micropillar Arrays. *BioNanoScience* **2014**, *4*, 349−355.
(58) Luo, S.; Yang, J.; Song, X.; Zhou, X.; Yu, L.; Sun, T.; Yu, C.; Huang, D.; Du, C.; Wei, D. Tunable-Sensitivity flexible pressure sensor based on graphene transparent electrode. *Solid-State Electron.* **2018**, *145*, 29−33.
(59) Dai, S.-W.; Gu, Y.-L.; Zhao, L.; Zhang, W.; Gao, C.-H.; Wu, Y.-X.; Shen, S.-C.; Zhang, C.; Kong, T.-T.; Li, Y.-T.; Gong, L.-X.; Zhang, G.-D.; Tang, L.-C. Bamboo-inspired mechanically flexible and electrically conductive polydimethylsiloxane foam materials with designed hierarchical pore structures for ultra-sensitive and reliable piezoresistive pressure sensor. *Composites, Part B* **2021**, *225*, No. 109243.
(60) Vianelli, A.; Candini, A.; Treossi, E.; Palermo, V.; Affronte, M. Observation of different charge transport regimes and large magnetoresistance in graphene oxide layers. *Carbon* **2015**, *89*, 188−196.
(61) Mott, N. F.; Davis, E. A. *Electronic processes in non-crystalline materials*; Clarendon Press; Oxford University Press: Oxford: New York, 1979.
(62) Muchharla, B.; Narayanan, T. N.; Balakrishnan, K.; Ajayan, P. M.; Talapatra, S. Temperature dependent electrical transport of disordered reduced graphene oxide. *2D Mater.* **2014**, *1*, No. 011008.
(63) Piatti, E.; Arbab, A.; Galanti, F.; Carey, T.; Anzi, L.; Spurling, D.; Roy, A.; Zhussupbekova, A.; Patel, K. A.; Kim, J. M.; Daghero, D.; Sordan, R.; Nicolosi, V.; Gonnelli, R. S.; Torrisi, F. Charge transport mechanisms in inkjet-printed thin-film transistors based on two-dimensional materials. *Nat. Electron.* **2021**, *4*, 893−905.
(64) El Hassan, M.; Dlimi, S.; Limouny, L.; El Oujdi, A.; Echchelh, A.; El Kaaouachi, A. Electrical transport phenomenon and variable range hopping conduction in reduced graphene oxide/polystyrene composites. *Mol. Cryst. Liq. Cryst.* **2022**, *726*, 82−89.
(65) Jimenez, M. J. M.; Oliveira, R. F.; Almeida, T. P.; Ferreira, R. C. H.; Bufon, C. C. B.; Rodrigues, V.; Pereira-da-Silva, M. A.; Gobbi, Â. L.; Piazzetta, M. H. O.; Riul, A., Jr. Charge carrier transport in defective reduced graphene oxide as quantum dots and nanoplatelets in multilayer films. *Nanotechnology* **2017**, *28*, No. 495711.
(66) Eda, G.; Mattevi, C.; Yamaguchi, H.; Kim, H.; Chhowalla, M. Insulator to Semimetal Transition in Graphene Oxide. *J. Phys. Chem. C* **2009**, *113*, 15768−15771.
(67) Chiu, F.-C. A Review on Conduction Mechanisms in Dielectric Films. *Adv. Mater. Sci. Eng.* **2014**, *2014*, No. 578168.
(68) Sakavičius, A.; Astromskas, G.; Lukša, A.; Bukauskas, V.; Nargelienė, V.; Matulaitienė, I.; Šetkus, A. Annealing Time Effect on Metal Graphene Contact Properties. *ECS J. Solid State Sci. Technol.* **2018**, *7*, M77.
(69) Amjadi, M.; Kyung, K. U.; Park, I.; Sitti, M. Stretchable, Skin-Mountable, and Wearable Strain Sensors and Their Potential Applications: A Review. *Adv. Funct. Mater.* **2016**, *26*, 1678−1698.

https://doi.org/10.1021/acs.chemmater.3c01191
Chem. Mater. 2023, 35, 6909−6919